DESY 95-052
March 1995

Measurement of the Cross Section for the Reaction $\gamma p \rightarrow J/\psi\, p$ with the ZEUS Detector at HERA

ZEUS Collaboration

Abstract

This paper reports the cross section measurements for the process $ep \rightarrow e\, J/\psi\, p$ for $Q^2 < 4$ GeV^2 at $\sqrt{s} = 296$ GeV, based on an integrated luminosity of about 0.5 pb^{-1}, using the ZEUS detector. The J/ψ was detected in its e^+e^- and $\mu^+\mu^-$ decay modes. The photoproduction cross section was measured to be $52^{+7}_{-12} \pm 10$ nb at an average γp centre of mass energy of 67 GeV and $71^{+13}_{-20} \pm 12$ nb at 114 GeV. The significant rise of the cross section compared to lower energy measurements is not in agreement with VDM models, but can be described by QCD inspired models if a rise in the gluon momentum density at low x in the proton is assumed.

The ZEUS Collaboration

M. Derrick, D. Krakauer, S. Magill, D. Mikunas, B. Musgrave, J. Repond, R. Stanek, R.L. Talaga, H. Zhang
Argonne National Laboratory, Argonne, IL, USA [p]

R. Ayad[1], G. Bari, M. Basile, L. Bellagamba, D. Boscherini, A. Bruni, G. Bruni, P. Bruni, G. Cara Romeo, G. Castellini[2], M. Chiarini, L. Cifarelli[3], F. Cindolo, A. Contin, M. Corradi, I. Gialas[4], P. Giusti, G. Iacobucci, G. Laurenti, G. Levi, A. Margotti, T. Massam, R. Nania, C. Nemoz,
F. Palmonari, A. Polini, G. Sartorelli, R. Timellini, Y. Zamora Garcia[1], A. Zichichi
University and INFN Bologna, Bologna, Italy [f]

A. Bargende, J. Crittenden, K. Desch, B. Diekmann[5], T. Doeker, M. Eckert, L. Feld, A. Frey, M. Geerts, G. Geitz[6], M. Grothe, T. Haas, H. Hartmann, D. Haun[5], K. Heinloth, E. Hilger,
H.-P. Jakob, U.F. Katz, S.M. Mari[4], A. Mass[7], S. Mengel, J. Mollen, E. Paul, Ch. Rembser, R. Schattevoy[8], D. Schramm, J. Stamm, R. Wedemeyer
Physikalisches Institut der Universität Bonn, Bonn, Federal Republic of Germany [c]

S. Campbell-Robson, A. Cassidy, N. Dyce, B. Foster, S. George, R. Gilmore, G.P. Heath, H.F. Heath, T.J. Llewellyn, C.J.S. Morgado, D.J.P. Norman, J.A. O'Mara, R.J. Tapper, S.S. Wilson, R. Yoshida
H.H. Wills Physics Laboratory, University of Bristol, Bristol, U.K. [o]

R.R. Rau
Brookhaven National Laboratory, Upton, L.I., USA [p]

M. Arneodo[9], L. Iannotti, M. Schioppa, G. Susinno
Calabria University, Physics Dept.and INFN, Cosenza, Italy [f]

A. Bernstein, A. Caldwell, N. Cartiglia, J.A. Parsons, S. Ritz[10], F. Sciulli, P.B. Straub, L. Wai, S. Yang, Q. Zhu
Columbia University, Nevis Labs., Irvington on Hudson, N.Y., USA [q]

P. Borzemski, J. Chwastowski, A. Eskreys, K. Piotrzkowski, M. Zachara, L. Zawiejski
Inst. of Nuclear Physics, Cracow, Poland [j]

L. Adamczyk, B. Bednarek, K. Jeleń, D. Kisielewska, T. Kowalski, E. Rulikowska-Zarębska,
L. Suszycki, J. Zając
Faculty of Physics and Nuclear Techniques, Academy of Mining and Metallurgy, Cracow, Poland [j]

A. Kotański, M. Przybycień
Jagellonian Univ., Dept. of Physics, Cracow, Poland [k]

L.A.T. Bauerdick, U. Behrens, H. Beier[11], J.K. Bienlein, C. Coldewey, O. Deppe, K. Desler, G. Drews, M. Flasiński[12], D.J. Gilkinson, C. Glasman, P. Göttlicher, J. Große-Knetter, B. Gutjahr, W. Hain, D. Hasell, H. Heßling, Y. Iga, P. Joos, M. Kasemann, R. Klanner, W. Koch, L. Köpke[13], U. Kötz, H. Kowalski, J. Labs, A. Ladage, B. Löhr, M. Löwe, D. Lüke, O. Mańczak, T. Monteiro[14], J.S.T. Ng, S. Nickel, D. Notz, K. Ohrenberg, M. Roco, M. Rohde, J. Roldán, U. Schneekloth, W. Schulz, F. Selonke, E. Stiliaris[15], B. Surrow, T. Voß, D. Westphal, G. Wolf, C. Youngman, J.F. Zhou
Deutsches Elektronen-Synchrotron DESY, Hamburg, Federal Republic of Germany

H.J. Grabosch, A. Kharchilava, A. Leich, M.C.K. Mattingly, A. Meyer, S. Schlenstedt, N. Wulff
DESY-Zeuthen, Inst. für Hochenergiephysik, Zeuthen, Federal Republic of Germany

G. Barbagli, P. Pelfer
University and INFN, Florence, Italy [f]

G. Anzivino, G. Maccarrone, S. De Pasquale, L. Votano
INFN, Laboratori Nazionali di Frascati, Frascati, Italy [f]

A. Bamberger, S. Eisenhardt, A. Freidhof, S. Söldner-Rembold[16], J. Schroeder[17], T. Trefzger
Fakultät für Physik der Universität Freiburg i.Br., Freiburg i.Br., Federal Republic of Germany [c]

N.H. Brook, P.J. Bussey, A.T. Doyle[18], J.I. Fleck[4], D.H. Saxon, M.L. Utley, A.S. Wilson
Dept. of Physics and Astronomy, University of Glasgow, Glasgow, U.K. [o]

A. Dannemann, U. Holm, D. Horstmann, T. Neumann, R. Sinkus, K. Wick
Hamburg University, I. Institute of Exp. Physics, Hamburg, Federal Republic of Germany [c]

E. Badura[19], B.D. Burow[20], L. Hagge, E. Lohrmann, J. Mainusch, J. Milewski, M. Nakahata[21], N. Pavel, G. Poelz, W. Schott, F. Zetsche
Hamburg University, II. Institute of Exp. Physics, Hamburg, Federal Republic of Germany [c]

T.C. Bacon, I. Butterworth, E. Gallo, V.L. Harris, B.Y.H. Hung, K.R. Long, D.B. Miller, P.P.O. Morawitz, A. Prinias, J.K. Sedgbeer, A.F. Whitfield
Imperial College London, High Energy Nuclear Physics Group, London, U.K. [o]

U. Mallik, E. McCliment, M.Z. Wang, S.M. Wang, J.T. Wu, Y. Zhang
University of Iowa, Physics and Astronomy Dept., Iowa City, USA [p]

P. Cloth, D. Filges
Forschungszentrum Jülich, Institut für Kernphysik, Jülich, Federal Republic of Germany

S.H. An, S.M. Hong, S.W. Nam, S.K. Park, M.H. Suh, S.H. Yon
Korea University, Seoul, Korea [h]

R. Imlay, S. Kartik, H.-J. Kim, R.R. McNeil, W. Metcalf, V.K. Nadendla
Louisiana State University, Dept. of Physics and Astronomy, Baton Rouge, LA, USA [p]

F. Barreiro[22], G. Cases, R. Graciani, J.M. Hernández, L. Hervás[22], L. Labarga[22], J. del Peso, J. Puga, J. Terron, J.F. de Trocóniz
Univer. Autónoma Madrid, Depto de Física Teóríca, Madrid, Spain [n]

G.R. Smith
University of Manitoba, Dept. of Physics, Winnipeg, Manitoba, Canada [a]

F. Corriveau, D.S. Hanna, J. Hartmann, L.W. Hung, J.N. Lim, C.G. Matthews, P.M. Patel, L.E. Sinclair, D.G. Stairs, M. St.Laurent, R. Ullmann, G. Zacek
McGill University, Dept. of Physics, Montréal, Québec, Canada [a, b]

V. Bashkirov, B.A. Dolgoshein, A. Stifutkin
Moscow Engineering Physics Institute, Mosocw, Russia [l]

G.L. Bashindzhagyan, P.F. Ermolov, L.K. Gladilin, Y.A. Golubkov, V.D. Kobrin, V.A. Kuzmin, A.S. Proskuryakov, A.A. Savin, L.M. Shcheglova, A.N. Solomin, N.P. Zotov
Moscow State University, Institute of Nuclear Physics, Moscow, Russia [m]

M. Botje, F. Chlebana, A. Dake, J. Engelen, M. de Kamps, P. Kooijman, A. Kruse, H. Tiecke, W. Verkerke, M. Vreeswijk, L. Wiggers, E. de Wolf, R. van Woudenberg
NIKHEF and University of Amsterdam, Netherlands [i]

D. Acosta, B. Bylsma, L.S. Durkin, K. Honscheid, C. Li, T.Y. Ling, K.W. McLean[23], W.N. Murray, I.H. Park, T.A. Romanowski[24], R. Seidlein[25]
Ohio State University, Physics Department, Columbus, Ohio, USA [p]

D.S. Bailey, G.A. Blair[26], A. Byrne, R.J. Cashmore, A.M. Cooper-Sarkar, D. Daniels[27], R.C.E. Devenish, N. Harnew, M. Lancaster, P.E. Luffman[28], L. Lindemann[4], J.D. McFall, C. Nath, V.A. Noyes, A. Quadt, H. Uijterwaal, R. Walczak, F.F. Wilson, T. Yip
Department of Physics, University of Oxford, Oxford, U.K. [o]

G. Abbiendi, A. Bertolin, R. Brugnera, R. Carlin, F. Dal Corso, M. De Giorgi, U. Dosselli, S. Limentani, M. Morandin, M. Posocco, L. Stanco, R. Stroili, C. Voci
Dipartimento di Fisica dell' Universita and INFN, Padova, Italy [f]

J. Bulmahn, J.M. Butterworth, R.G. Feild, B.Y. Oh, J.J. Whitmore[29]
Pennsylvania State University, Dept. of Physics, University Park, PA, USA [q]

G. D'Agostini, G. Marini, A. Nigro, E. Tassi
Dipartimento di Fisica, Univ. 'La Sapienza' and INFN, Rome, Italy [f]

J.C. Hart, N.A. McCubbin, K. Prytz, T.P. Shah, T.L. Short
Rutherford Appleton Laboratory, Chilton, Didcot, Oxon, U.K. [o]

E. Barberis, T. Dubbs, C. Heusch, M. Van Hook, B. Hubbard, W. Lockman, J.T. Rahn, H.F.-W. Sadrozinski, A. Seiden
University of California, Santa Cruz, CA, USA [p]

J. Biltzinger, R.J. Seifert, A.H. Walenta, G. Zech
Fachbereich Physik der Universität-Gesamthochschule Siegen, Federal Republic of Germany [c]

H. Abramowicz, G. Briskin, S. Dagan[30], A. Levy[31]
School of Physics,Tel-Aviv University, Tel Aviv, Israel [e]

T. Hasegawa, M. Hazumi, T. Ishii, M. Kuze, S. Mine, Y. Nagasawa, M. Nakao, I. Suzuki, K. Tokushuku, S. Yamada, Y. Yamazaki
Institute for Nuclear Study, University of Tokyo, Tokyo, Japan [g]

M. Chiba, R. Hamatsu, T. Hirose, K. Homma, S. Kitamura, Y. Nakamitsu, K. Yamauchi
Tokyo Metropolitan University, Dept. of Physics, Tokyo, Japan [g]

R. Cirio, M. Costa, M.I. Ferrero, L. Lamberti, S. Maselli, C. Peroni, R. Sacchi, A. Solano, A. Staiano
Universita di Torino, Dipartimento di Fisica Sperimentale and INFN, Torino, Italy [f]

M. Dardo
II Faculty of Sciences, Torino University and INFN - Alessandria, Italy [f]

D.C. Bailey, D. Bandyopadhyay, F. Benard, M. Brkic, M.B. Crombie, D.M. Gingrich[32], G.F. Hartner, K.K. Joo, G.M. Levman, J.F. Martin, R.S. Orr, C.R. Sampson, R.J. Teuscher
University of Toronto, Dept. of Physics, Toronto, Ont., Canada [a]

C.D. Catterall, T.W. Jones, P.B. Kaziewicz, J.B. Lane, R.L. Saunders, J. Shulman
University College London, Physics and Astronomy Dept., London, U.K. [o]

K. Blankenship, B. Lu, L.W. Mo
Virginia Polytechnic Inst. and State University, Physics Dept., Blacksburg, VA, USA [q]

W. Bogusz, K. Charchuła, J. Ciborowski, J. Gajewski, G. Grzelak, M. Kasprzak, M. Krzyżanowski, K. Muchorowski, R.J. Nowak, J.M. Pawlak, T. Tymieniecka, A.K. Wróblewski, J.A. Zakrzewski, A.F. Żarnecki
Warsaw University, Institute of Experimental Physics, Warsaw, Poland [j]

M. Adamus
Institute for Nuclear Studies, Warsaw, Poland [j]

Y. Eisenberg[30], U. Karshon[30], D. Revel[30], D. Zer-Zion
Weizmann Institute, Nuclear Physics Dept., Rehovot, Israel [d]

I. Ali, W.F. Badgett, B. Behrens, S. Dasu, C. Fordham, C. Foudas, A. Goussiou, R.J. Loveless, D.D. Reeder, S. Silverstein, W.H. Smith, A. Vaiciulis, M. Wodarczyk
University of Wisconsin, Dept. of Physics, Madison, WI, USA [p]

T. Tsurugai
Meiji Gakuin University, Faculty of General Education, Yokohama, Japan

S. Bhadra, M.L. Cardy, C.-P. Fagerstroem, W.R. Frisken, K.M. Furutani, M. Khakzad, W.B. Schmidke
York University, Dept. of Physics, North York, Ont., Canada [a]

[1] supported by Worldlab, Lausanne, Switzerland
[2] also at IROE Florence, Italy
[3] now at Univ. of Salerno and INFN Napoli, Italy
[4] supported by EU HCM contract ERB-CHRX-CT93-0376
[5] now a self-employed consultant
[6] on leave of absence
[7] now at Institut für Hochenergiephysik, Univ. Heidelberg
[8] now at MPI Berlin
[9] now also at University of Torino
[10] Alfred P. Sloan Foundation Fellow
[11] presently at Columbia Univ., supported by DAAD/HSPII-AUFE
[12] now at Inst. of Computer Science, Jagellonian Univ., Cracow
[13] now at Univ. of Mainz
[14] supported by DAAD and European Community Program PRAXIS XXI
[15] supported by the European Community
[16] now with OPAL Collaboration, Faculty of Physics at Univ. of Freiburg
[17] now at SAS-Institut GmbH, Heidelberg
[18] also supported by DESY
[19] now at GSI Darmstadt
[20] also supported by NSERC
[21] now at Institute for Cosmic Ray Research, University of Tokyo
[22] on leave of absence at DESY, supported by DGICYT
[23] now at Carleton University, Ottawa, Canada
[24] now at Department of Energy, Washington
[25] now at HEP Div., Argonne National Lab., Argonne, IL, USA
[26] now at RHBNC, Univ. of London, England
[27] Fulbright Scholar 1993-1994
[28] now at Cambridge Consultants, Cambridge, U.K.
[29] on leave and partially supported by DESY 1993-95
[30] supported by a MINERVA Fellowship
[31] partially supported by DESY
[32] now at Centre for Subatomic Research, Univ.of Alberta, Canada and TRIUMF, Vancouver, Canada

[a] supported by the Natural Sciences and Engineering Research Council of Canada (NSERC)
[b] supported by the FCAR of Québec, Canada
[c] supported by the German Federal Ministry for Research and Technology (BMFT)
[d] supported by the MINERVA Gesellschaft für Forschung GmbH, and by the Israel Academy of Science
[e] supported by the German Israeli Foundation, and by the Israel Academy of Science
[f] supported by the Italian National Institute for Nuclear Physics (INFN)
[g] supported by the Japanese Ministry of Education, Science and Culture (the Monbusho) and its grants for Scientific Research
[h] supported by the Korean Ministry of Education and Korea Science and Engineering Foundation
[i] supported by the Netherlands Foundation for Research on Matter (FOM)
[j] supported by the Polish State Committee for Scientific Research (grant No. SPB/P3/202/93) and the Foundation for Polish- German Collaboration (proj. No. 506/92)
[k] supported by the Polish State Committee for Scientific Research (grant No. PB 861/2/91 and No. 2 2372 9102, grant No. PB 2 2376 9102 and No. PB 2 0092 9101)
[l] partially supported by the German Federal Ministry for Research and Technology (BMFT)
[m] supported by the German Federal Ministry for Research and Technology (BMFT), the Volkswagen Foundation, and the Deutsche Forschungsgemeinschaft
[n] supported by the Spanish Ministry of Education and Science through funds provided by CICYT
[o] supported by the Particle Physics and Astronomy Research Council
[p] supported by the US Department of Energy
[q] supported by the US National Science Foundation

1 Introduction

Elastic photoproduction of J/ψ (γp$\rightarrow$ J/ψp) is particularly interesting as the production cross section can be calculated as a function of the γp centre of mass (c.m.) energy, W, both using the Vector Dominance Model[1] (VDM) extended to the heavy quarks [2, 3, 4], and, because of the large value of the J/ψ mass ($M_{J/\psi}$), with QCD inspired models[5, 6]. Figures 1a and 1b show the elastic J/ψ photoproduction mechanisms according to VDM and QCD inspired models, respectively. A characteristic of these QCD inspired models is that the cross section is proportional to the square of the proton's gluon momentum density. The typical x range probed here, where x ($\simeq M^2_{J/\psi}/W^2$) is the fraction of the proton momentum carried by the gluon, is approximately 5×10^{-3} to 5×10^{-4}, corresponding to a W range between 40 and 140 GeV. For gluon distributions increasing at low x, the QCD approaches predict much higher cross sections than those from the VDM in this W region.

Previous measurements of the photoproduction of J/ψ are available in the W range between 4 GeV and 28 GeV[7, 8]. However, some results include elastic as well as other production mechanisms of the J/ψ. The H1 experiment has also reported[9] a J/ψ photoproduction cross section measurement at an average c.m. energy of 90 GeV, that contains an unknown contribution from inelastic J/ψ photoproduction.

This paper reports the measurements of photoproduction cross sections of elastically produced J/ψ's in the reaction ep $\rightarrow$ e J/ψ p, followed by J/$\psi \rightarrow e^+e^-$or J/$\psi \rightarrow \mu^+\mu^-$, with the ZEUS detector. The present data sample contains events with $Q^2 < 4$ GeV^2, with a median $Q^2 \sim 10^{-3}$ GeV^2, in the W range between 40 and 140 GeV. Neither the scattered electron nor the proton is detected in this measurement. The contribution of J/ψ production where the proton diffractively dissociated is subtracted to obtain the elastic photoproduction cross section.

2 HERA

The data presented were collected during the 1993 running period of HERA and represent an integrated luminosity of about 0.5 pb^{-1}. HERA operated in 1993 with an electron beam energy of 26.7 GeV and a proton beam energy of 820 GeV. A total of 84 colliding electron and proton bunches was used; in addition 10 electron and 6 proton unpaired bunches were used for background studies. The time between bunch crossings at HERA is 96 ns. A typical instantaneous luminosity of $\sim 6 \times 10^{29}$cm^{-2}s^{-1} was delivered.

3 The ZEUS detector

The ZEUS detector[10] is a hermetic, general purpose magnetic detector with a tracking region surrounded by a high resolution calorimeter followed in turn by a backing calorimeter and the muon detector. A short description of the components relevant to this analysis is given here. They are the vertex detector[11], the central-tracking detector[12], the uranium-scintillator calorimeter[13] and the barrel and rear muon detectors[14].

Charged particles are measured by the ZEUS inner tracking detectors, which operate in a magnetic field of 1.43 T provided by a thin superconducting coil. Immediately surrounding the

beampipe is the vertex detector (VXD) consisting of 120 radial cells, each with 12 sense wires. It uses a slow drift velocity gas and the presently achieved resolution in the XY[1] plane is 50 μm in the central region of a cell and 150 μm near the edges. Surrounding the VXD is the central tracking detector (CTD) which consists of 72 cylindrical drift chamber layers, arranged in 9 'superlayers'. With our present calibration of the chamber, the resolution of the CTD is around 260 μm. The resolution in transverse momentum for tracks going through all superlayers is $\sigma(p_T)/p_T \approx \sqrt{(0.005)^2\, p_T^2 + (0.016)^2}$ where p_T is in GeV. The single hit efficiency is greater than 95%. The efficiency for assigning hits to tracks depends on several factors: very low p_T tracks suffer large systematic effects which reduce the probability of hits being assigned to them, and the 45° inclination of the drift cells also introduces an asymmetry between positive and negative tracks. Nevertheless, the track reconstruction efficiency for tracks with $p_T > 0.1$ GeV is greater than 95%. Using the combined data from the VXD and CTD, resolutions of 0.4 cm in Z and 0.1 cm in radius in the XY plane are obtained for the primary vertex reconstruction. From Gaussian fits to the Z vertex distribution, the r.m.s. spread is found to be 10.5 cm, in agreement with the expectation based on the HERA proton bunch length.

The high resolution uranium-scintillator calorimeter (CAL) covers the polar angle range between $2.2° < \theta < 176.5°$, where $\theta = 0°$ is the proton beam direction. It consists of three parts: the rear calorimeter (RCAL), covering the backward pseudorapidity[2] range ($-3.4 < \eta < -0.75$); the barrel calorimeter (BCAL) covering the central region ($-0.75 < \eta < 1.1$); and the forward calorimeter (FCAL) covering the forward region ($1.1 < \eta < 3.8$). The calorimeter parts are subdivided into towers which in turn are subdivided longitudinally into electromagnetic (EMC) and hadronic (HAC) sections. The sections are subdivided into cells, each of which is viewed by two photomultiplier tubes. Under test beam conditions the CAL has an energy resolution, in units of GeV, of $\sigma_E = 0.35\sqrt{E(\mathrm{GeV})}$ for hadrons and $\sigma_E = 0.18\sqrt{E(\mathrm{GeV})}$ for electrons. The CAL also provides a time resolution of better than 1 ns for energy deposits greater than 4.5 GeV, and this timing is used for background rejection.

The muon detectors, placed outside the calorimeter, are also divided into three sections, covering the forward, barrel and rear regions. In the barrel and rear regions limited streamer tube (LST) chambers before (inner) and after (outer) an 80 cm thick magnetized iron yoke are used. Only the inner chambers of the barrel and rear muon detectors (BMUI and RMUI) were used for the present analysis. The BMUI and the RMUI cover the polar angles between $34° \leq \theta \leq 135°$ and $134° \leq \theta < 171°$, respectively. Each chamber has 2 double layers of LST; spatial resolutions of 1 and 3 mm have been obtained along the direction of the tube axis and perpendicular to it, respectively.

A set of four scintillation counters (C5) in two planes interleaved with a 3 mm Pb foil immediately behind the RCAL at approximately Z = −3 m partially surrounds the beampipe. The C5 counter measures the timing of both beams and also tags events from proton-gas interactions. A vetowall (VETO), consisting of two layers of scintillator on either side of an 87 cm thick iron wall centred at Z = −7.3 m, was also used to tag and reject off-axis beam particles.

The ep luminosity was measured from the rate of the Bethe-Heitler process ($ep \to e\gamma p$) by counting the final state photons in the luminosity monitor.

[1] The ZEUS detector uses a right-handed coordinate system where the Z axis points in the direction of the proton beam (forward direction) and the X axis is horizontal, pointing towards the centre of HERA, with the nominal Interaction Point (IP) at (0,0,0).

[2] Pseudorapidity is defined as $\eta = -\ln[\tan(\frac{\theta}{2})]$.

4 Kinematics

The kinematics of the elastic process ep $\rightarrow$ e J/ψ p are described below. The incoming and outgoing electron four-momenta are denoted by k and k', respectively, while the four-momentum of the virtual photon is $q = k - k'$; $Q^2 \equiv -q^2$. If $P(P')$ is the incoming(outgoing) proton four-momentum, and $P_{\mathrm{J}/\psi}$ is the J/ψ four-momentum, then the squared four-momentum transfer t is defined as

$$t = (P - P')^2 = (q - P_{\mathrm{J}/\psi})^2.$$

For $Q^2 \simeq 0$, $t \simeq -p_{T\mathrm{J}/\psi}^2$, where $p_{T\mathrm{J}\psi}$ is the transverse momentum carried by the J/ψ. W is given by $W^2 = (P+q)^2$. The Lorentz scalar y is defined as $P \cdot q / P \cdot k$, and can be approximated as:

$$y \simeq (E - p_Z)_{\mathrm{J}/\psi}/2E_e, \quad \text{and} \quad W^2 = sy \simeq 4E_e E_p y \simeq 2(E - p_Z)_{\mathrm{J}/\psi} E_p,$$

where E_e denotes the electron beam energy, E_p is the proton beam energy, $\sqrt{s}$ is the ep c.m. energy, and E is the energy and p_Z is the Z component of the momentum of the J/ψ.

5 Trigger and preselection

5.1 Trigger

The J/ψ was identified from its leptonic decay modes. The momenta of the decay leptons from the J/ψ's in the observed kinematic range are low ($\sim$ 1.5 GeV). To trigger on these low momentum lepton tracks in the high background environment of HERA, where the typical background rate from beam-gas interactions exceeds 10 KHz, requires a very selective trigger.

ZEUS uses a three level trigger scheme[10]. The first level trigger (FLT) is built as a deadtime-free pipeline. The triggering on the leptons from the decay of the J/ψ used the CTD, CAL and the muon chambers and is described below.

Events with low momentum electrons were selected two ways by the FLT:

- by requiring a minimum energy deposit of 660 MeV in the EMC. To reduce background, a total CAL energy deposit greater than 2 GeV or a total energy deposit in the FCAL, excluding the region adjacent to the beampipe, greater than 2.5 GeV were required. In addition, one to three track segments in the innermost superlayer of the CTD were required,
- by requiring a minimum energy deposit of 464 MeV in REMC and any track segment in the innermost CTD superlayer.

In both of these cases, events were vetoed if the energy deposit in the FCAL region immediately surrounding the beam pipe exceeded 3.75 GeV to reduce the background from proton gas interactions.

The analysis of the muon decay mode used the inclusive muon triggers; events with low momentum muons were selected by the FLT in one of two ways by requiring:

- hits in the RMUI accompanied by an energy deposit of at least 464 MeV in the RCAL,
- hits in the BMUI accompanied by an energy deposit of at least 464 MeV in the CAL.

The trigger used only the inner muon chambers to maximize the acceptance.

All four of these triggers also required at least one CTD track segment pointing towards the IP, along with the appropriate VETO and C5 signals to ascertain that the event originated from the IP.

The second level trigger (SLT) reduced the beam related background further by making use of the subnanosecond time resolution of the CAL and by requiring that the energy deposits in the CAL were in time with the bunch crossing.

The third level trigger (TLT) ran on a farm of processors; an event was flagged by the TLT as a J/ψ candidate if either of the following criteria was satisfied:

• Electron Mode: a fast electron identification was carried out by using information from the CTD and CAL. Electrons were identified by an energy deposit in the EMC of at least 90% of the cluster energy, where a cluster is defined as a number of contiguous cells with energy deposit. The tracks from the CTD were extrapolated towards the CAL and matched[3] with a cluster in order to determine the energy deposited in the calorimeter by that track. An event was accepted if it had a pair of oppositely charged tracks, each associated with such an electron cluster and each with a momentum exceeding 0.5 GeV and p_T higher than 0.4 GeV. The track reconstruction in the TLT used the 'Z-by-timing' information available from the first three axial superlayers of the CTD. Additional requirements imposed on the events to remove beam-gas interactions were $\Sigma_i p_{Zi}/\Sigma_i E_i \leq 0.94$ and $\Sigma_i(E_i - p_{Zi}) \leq 100$ GeV, where the sums are over all calorimeter cells.

• Muon Mode: for an event with a muon FLT trigger, a match between track segments from the CTD and the inner muon chambers was required, with energy deposits compatible with those from a minimum ionizing particle in the calorimeter EMC and HAC sections. A track with a minimum p_T of 1 GeV in the barrel region or a minimum momentum of 1 GeV in the rear region was flagged as an inclusive muon trigger and satisfied the TLT requirement.

5.2 Preselection

All events satisfying the TLT criteria were reconstructed offline where the more refined information from the CTD was used for tracking. The event samples were then divided into an electron sample based on kinematics and track-CAL cluster matching, and a muon sample based on muon identification by the muon chambers.

• Electron Mode: events with two oppositely charged tracks, each with $p_T \geq 0.5$ GeV, where one of the two had a minimum momentum of 1 GeV, were selected. The tracks, which were required to originate from the event vertex, were matched to a CAL cluster as in the TLT, and were selected if the invariant e^+e^- mass was between 2 and 4 GeV. This data sample contained 2021 events from a total luminosity of 486 nb^{-1}.

[3]The distance of closest approach between the extrapolated track and the centre of the cluster was required to be less than 30 cm.

• Muon Mode: Cosmic ray events, the biggest background in the muon sample, were substantially reduced by using the time difference between the upper and the lower halves of the calorimeter. Again, events with two oppositely charged tracks, each with $p_T \geq 0.5$ GeV, originating from a vertex, were retained. A further reduction in beam gas contamination was achieved by requiring $\Sigma_i p_{Zi}/\Sigma E_i \leq 0.96$, where the sum was over all calorimeter cells. This sample contained 456 events from a total luminosity of 490 nb^{-1}.

6 Analysis

6.1 The J/ψ signal

In order to ensure a high quality of track reconstruction, for both data samples only tracks within the pseudorapidity range $|\eta| < 1.5$ were considered. In addition, the total energy in the CAL, apart from the energy deposited by the two leptons from the J/ψ candidate, was required to be less than 1.0 GeV. This criterion was imposed to reject inelastic events. Only events where the acceptance was high (the W range between 40 and 140 GeV) were retained.

• Electron decay mode: a total of 136 events satisfied these criteria with 72 events in the invariant mass range 2.85 - 3.25 GeV. The resulting e^+e^- invariant mass distribution ($M_{e^+e^-}$) is shown in Fig. 2a. A clear peak is visible at the J/ψ mass. The asymmetric shape is attributed to energy loss by the bremsstrahlung process in the material encountered by the decay electrons. The same asymmetry was observed in the reconstructed events from the Monte Carlo study described below. A maximum likelihood fit to the e^+e^- mass spectrum was performed using a Gaussian shape convoluted with a bremsstrahlung function to account for the energy loss; a second order polynomial in $M_{e^+e^-}$ was used to describe the background. The processes contributing to the background are described in section 6.3. In this fit, the fraction of events undergoing bremsstrahlung was constrained to be that determined from the Monte Carlo study described below. The mass (3.08 ± 0.01 GeV) and the resolution (38 ± 10 MeV), used as free parameters in the fit, were in agreement with the predictions of the Monte Carlo simulation. The fit, shown in Fig. 2a, yields 72 ± 9 events for the J/ψ signal.

• Muon decay mode: the muon data sample still contained some contamination from cosmic ray muons. These were identified and removed by applying a collinearity criterion. A total of 45 events satisfied the selection criteria in the invariant mass range between 2 and 4 GeV, with 35 events in the invariant mass range between 2.85 and 3.25 GeV. Figure 2b shows the invariant mass spectrum: a clear peak at the J/ψ mass is observed. The mass spectrum was fitted with the combination of a Gaussian and a flat background, shown in Fig. 2b. The fitted mass (3.08 ± 0.01 GeV) and the resolution (61 ± 13 MeV) were again in agreement with the Monte Carlo expectations. The fit yielded 32 ± 6 signal events.

6.2 Monte Carlo simulation and acceptance

Elastic J/ψ production was simulated with the DIPSI[15] and the EPJPSI[16] generators. The model used by DIPSI assumes that the exchanged photon fluctuates into a $q\bar{q}$ pair which then interacts with the proton via the exchange of a pomeron described in terms of a gluon ladder[5].

The model is based on a perturbative QCD calculation in the leading log approximation. The hard scale in this model is taken to be $\mu^2 \simeq M^2_{J/\psi}/4 \simeq 2.5$ GeV^2. The gluon momentum density of the proton, used as input in the DIPSI Monte Carlo, was $\propto x^{-0.4}$. The EPJPSI generator assumes pomeron exchange for the elastic J/ψ production. Two different models of the pomeron were used. In the first model, the pomeron consists of two gluons, and one of the gluons interacts with the c$\bar{\text{c}}$ state into which the photon has fluctuated; the J/ψ is formed from the c$\bar{\text{c}}$ and the remaining gluon of the pomeron. In the second model, the pomeron is without a structure, and it interacts with the photon as a whole to form the J/ψ.

Events were generated in the W range between 30 and 200 GeV and between the minimum allowed value of Q^2 ($\simeq 10^{-10}$ GeV^2) and 4 GeV^2. The events were then passed through the standard ZEUS detector and trigger simulation programs, and processed with the same reconstruction and analysis programs as the data. The distributions of the reconstructed kinematic quantities obtained using DIPSI were in good agreement with those from the data. The overall acceptance (including the geometric acceptance, detector, trigger and reconstruction efficiencies) was then obtained using DIPSI as the ratio of the number of accepted Monte Carlo events to the number generated in the selected kinematic range of W between 40 and 140 GeV. Events generated with EPJPSI reproduced some aspects of the data well and were used in the study of systematic uncertainties in the acceptance determination. Table 1 shows the acceptances[4] in various W ranges determined for each decay mode.

6.3 Background

Two types of background contributions were considered: the first is a continuum background present over the complete mass range, which was already subtracted in obtaining the number of signal events from the fit; the second type is J/ψ production through proton dissociation or other inelastic production processes.

• Continuum background: the Bethe-Heitler process produces lepton pairs from photon-photon scattering where the electron and the proton each radiates a photon. The invariant mass spectrum of the lepton pair, either e^+e^-or $\mu^+\mu^-$, typically forms a continuum with a maximum at low masses. The contribution from this process was obtained by generating Monte Carlo events using the generator LPAIR[17]. These events were treated the same way as those generated by DIPSI. The hatched regions in Fig. 2a and 2b show the LPAIR events, normalized to the appropriate ep luminosity, which survived all the selection criteria. In the mass region between 2.85 and 3.25 GeV, the background from this process in each mode is $\sim 8.5\%$.

For the electron decay mode, a second source of continuum background was responsible for the difference between the quadratic polynomial (dashed curve) and the two photon process shown in Fig. 2a (hatched area). After studies with data and Monte Carlo, this was determined to be from pion contamination. One or both of the electron candidates could be misidentified pions; the probability of misidentification decreases with increasing momentum. In the mass range between 2 and 4 GeV, the background from the pion contamination is comparable to that from the two-photon process.

[4]The efficiency of the CAL trigger threshold for the muon decay mode was found to be 90%; this has been included in the acceptance values. Also included is an additional factor of 0.9 for the muon chamber efficiency.

• the proton dissociation process in reactions like ep $\rightarrow$ e J/ψ X, where X was undetected, can also contribute to the observed J/ψ signal, as the outgoing proton is not observed. This background was estimated by removing the criterion that the energy deposited in CAL, excluding that from the J/ψ decay leptons, be less than 1 GeV. A total of four events in the electron mode and three events in the muon mode were observed with CAL close to the proton direction; these are candidates for J/ψ production accompanied by proton dissociation. Monte Carlo events simulating this process were generated with PYTHIA[18]; the mass distribution of the diffractive system X was parametrised as $d\sigma/dM_X{}^2 \sim M_X{}^{-n}$ where n was varied[5] between 2 and 3. These Monte Carlo events were analysed in the same way as the data. For $n = 2.5$, the proton dissociative contamination in the J/ψ signal was estimated to be 17%, by comparing the number of events with extra energy in CAL from this Monte Carlo sample with the seven events from the data. The fraction of proton dissociative contamination determined was $(17^{+8}_{-5} \pm 10)\%$, where the first uncertainty is statistical, obtained from the electron and the muon modes together, and the second uncertainty is systematic, observed from the variation of n between 2 and 3 in the Monte Carlo. The cross section for the elastic process was thus obtained by subtracting 17% from the J/ψ signal, independent of W.

• the contribution from the photon-gluon fusion process was determined from Monte Carlo studies using HERWIG[21] and EPJPSI[16]. Possible contributions from $\psi(3685)$ production and processes where the photon undergoes diffractive dissociation e.g., $\gamma \rightarrow$ J/ψ X, where X was not detected, were also considered. The total contribution from these processes was found to be negligible and a systematic uncertainty of 3% was assigned to it.

7 Results

7.1 ep cross section

The electroproduction cross section, $\sigma_{\rm ep}$, is calculated as: $\sigma_{\rm ep} = \frac{1}{A} \times \frac{1}{Br} \times \frac{1}{\mathcal{L}} \times N$, where N denotes the number of J/ψ signal events, A the acceptance, $\mathcal{L}$ the integrated luminosity, and Br the leptonic branching fraction of J/ψ[22], namely $(5.99 \pm 0.25)\%$ for $e^+e^-$and $(5.97 \pm 0.25)\%$ for $\mu^+\mu^-$. Subtracting the 17% contribution to the J/ψ signal from the proton dissociation process, we obtain for the elastic cross section for the process ep $\rightarrow$ e J/ψ p for $Q^2 < 4$ GeV^2 and $\sqrt{s} = 296$ GeV in the W range between 40 and 140 GeV: $\sigma_{\rm ep} = 6.6^{+1.0}_{-1.3}$ nb, and $\sigma_{\rm ep} = 6.2^{+1.1}_{-1.6}$ nb, from the electron and the muon decay modes, respectively. The errors are statistical.

Figure 3 shows the $\mathrm{d}\sigma_{\rm ep}/\mathrm{d}p^2_{T\mathrm{J}/\psi}$ differential cross section for both decay channels combined after the background subtractions. An exponential fit of the form $\exp(-bp^2_{T\mathrm{J}/\psi})$ to the distribution in the range $0 \leq p^2_{T\mathrm{J}/\psi} \leq 1$ GeV^2 yields a slope b of 3.7 ± 1.0 GeV^{-2}, while a fit in the range $0 \leq p^2_{T\mathrm{J}/\psi} \leq 0.75$ GeV^2 gives a slope b of 4.5 ± 1.4 GeV^{-2}, where the statistical and the systematic errors have been added in quadrature. The acceptance in these $p^2_{T\mathrm{J}/\psi}$ ranges was constant within 15%. As noted earlier, for $Q^2 \simeq 0$, $p^2_{T\mathrm{J}/\psi}$ approximates $|t|$. Taking into account the Q^2 dependence, the slope of the $|t|$ distribution obtained from the Monte Carlo is ~ 0.5

[5]The CDF Collaboration reported a measurement of $n = 2.20 \pm 0.03$ at $\sqrt{s} = 1800$ GeV[19], in agreement with Regge theory predictions[20], which is well within the range between 2 and 3 considered.

unit higher than the slope obtained from the $p^2_{T\mathrm{J}/\psi}$ distribution, in the $p^2_{T\mathrm{J}/\psi}$ ranges described above.

In order to determine the cross section dependence on W, the data samples were divided into two W ranges: $40 \leq W \leq 90$ GeV and $90 \leq W \leq 140$ GeV. Table 1 lists the elastic cross sections from each W range after subtracting the backgrounds, along with the numbers of events and the acceptances.

Table 1: Acceptance and cross sections

W range (GeV)	40 - 90		90 - 140	
decay mode	$\mathrm{J}/\psi \to e^+e^-$	$\mathrm{J}/\psi \to \mu^+\mu^-$	$\mathrm{J}/\psi \to e^+e^-$	$\mathrm{J}/\psi \to \mu^+\mu^-$
acceptance	0.39	0.11	0.22	0.19
signal events	44^{+7}_{-11}	15^{+4}_{-5}	16 ± 4	12^{+5}_{-6}
σ_{ep}(nb)	$3.9^{+0.6}_{-1.0}\pm 0.7$	$4.7^{+1.2+0.9}_{-1.6-1.0}$	$2.5\pm 0.6\pm 0.4$	$2.2^{+0.9+0.4}_{-1.0-0.5}$
integrated photon flux	0.077		0.033	
$\sigma_{\gamma\mathrm{p}}$(nb)	$50^{+8}_{-13}\pm 10$	61^{+16+14}_{-20-14}	$76^{+19}_{-24} \pm 13$	65^{+16+13}_{-33-14}
$\langle W \rangle$ (GeV)	67 ± 11		114 ± 9	
$\sigma_{\gamma p}$ (nb)	$52^{+7}_{-12} \pm 10$		$71^{+13}_{-20} \pm 12$	

7.2 Systematic uncertainties

The summary of the uncertainties from various sources is reported in Table 2. The polarization of the J/ψ was not measured and the angular distribution of the decay leptons was varied from flat to the form $1 + \cos^2\theta^*$, where θ^* is the decay angle of the leptons in the J/ψ rest frame with respect to the J/ψ lab momentum. This could affect the acceptance by up to 5%. No uncertainty was attributed to the W calculation, as the resolution in W is of the order of 1%. The variation in acceptance from the modeling of the W dependence was calculated using the different Monte Carlo generators described in section 6.2; an uncertainty of 9% was assigned to each of the decay modes. The uncertainty in acceptance from the variation in the gluon density was included in modeling the W distribution in the Monte Carlo simulations. The computation of the muon chamber efficiency added an asymmetric uncertainty as shown in Table 2. The uncertainty from the track multiplicity determination was observed to be 5%. The energy deposit in CAL was obtained after the uranium noise subtraction[13]. This led to a 4% uncertainty. The uncertainty due to the calorimeter trigger thresholds for the muon decay channel was 10%. For the electron mode, the energy requirement for triggering was far enough above the threshold that only a maximum of 5% variation could be observed in the efficiency determination.

An uncertainty of 10% was attributed to the subtraction of the proton dissociation process, and a 3% uncertainty was added to account for contributions from other possible inelastic processes to the signal, referred to as feed-in from other modes, as discussed in section 6.3. A total uncertainty of 17% for the electron mode and $^{+20\%}_{-21\%}$ for the muon mode in the electroproduction cross section was thus obtained by adding all contributions in quadrature.

Table 2: Systematic uncertainties for the ep $\rightarrow$ e J/ψ p cross section measurement

uncertainties	$J/\psi \rightarrow e^+e^-$	$J/\psi \rightarrow \mu^+\mu^-$
branching fraction	4 %	4 %
luminosity	3.3 %	3.3 %
J/ψ decay angular distribution	5 %	5 %
W dependence	9 %	9 %
muon chamber efficiency		+5 % −9 %
track multiplicity	5 %	5 %
$\leq$1 GeV energy requirement	4 %	4 %
CAL trigger threshold	5 %	10 %
proton dissociation subtraction	10 %	10 %
feed-in from other modes	3 %	3 %
total	17 %	+20 % −21 %

7.3 Photoproduction cross section

The photon-proton cross section $\sigma_{\gamma p \rightarrow J/\psi p}$ is obtained from the corresponding electron-proton cross section by using the relation :

$$\sigma_{ep}(s) = \int_{y_{min}}^{y_{max}} dy \int_{Q^2_{min}}^{Q^2_{max}} dQ^2 \cdot \Phi(y, Q^2) \cdot \sigma_{\gamma^* p}(y, Q^2),$$

where

$$\Phi(y, Q^2) = \frac{\alpha}{2\pi} \frac{1}{yQ^2} [1 + (1-y)^2 - \frac{2m_e^2 y^2}{Q^2}]$$

is the photon flux factor[23], $Q^2_{min} = m_e^2 \frac{y^2}{1-y}$, $Q^2_{max} = 4$ GeV^2 and m_e is the electron mass. Since the median $Q^2 \approx 10^{-3}$ GeV^2 is very small, we can neglect the longitudinal contribution and the Q^2 dependence of $\sigma_{\gamma^* p}$. The γp cross section is then obtained as the ratio of the measured ep cross section and the photon flux factor Φ integrated over the Q^2 and y range covered by the measurement. This procedure assumes that $\sigma_{\gamma p}$ is independent of y in the range of the measurement. As this dependence is not known a priori, the above calculation was repeated assuming a rise of $\sigma_{\gamma p}(W)$ proportional to W ($= \sqrt{sy}$). An increase of 10% in the resulting cross section was found at $\langle W \rangle = 67$ GeV and less than 2% at $\langle W \rangle = 114$ GeV. These have been added in the systematic uncertainty in the photoproduction cross section measurements. The cross sections and the integrated photon flux in the different W ranges are summarized in Table 1. The first uncertainty quoted for the cross sections is statistical and the second is systematic. Combining results from the two leptonic decay modes, the measured J/ψ photoproduction elastic cross sections are :

$$\begin{aligned} \sigma_{\gamma p \rightarrow J/\psi p} &= 52^{+7}_{-12} \pm 10 \; nb \quad for \; \langle W \rangle = 67 \text{ GeV and} \\ \sigma_{\gamma p \rightarrow J/\psi p} &= 71^{+13}_{-20} \pm 12 \; nb \quad for \; \langle W \rangle = 114 \text{ GeV}. \end{aligned}$$

The first error is the weighted error of the uncertainty specific to each decay mode where this uncertainty is obtained by combining the statistical error and the systematic error unique to the decay mode in quadrature; this error was used to obtain the weighted combined cross section. The second error is the systematic error common to both decay modes.

8 Discussion

Figure 4 displays a compilation of the J/ψ elastic photoproduction cross section measurements[8]. The compilation includes only results from the fixed target experiments which measured the recoil proton. The elastic J/ψ photoproduction measurements by ZEUS are also shown, where the elastic cross section has been obtained by subtracting the proton dissociative production of the J/ψ. A significant rise of the J/ψ cross section with the c.m. energy is visible.

Theoretical predictions based on Regge-type and QCD inspired models are also shown in Fig. 4. The solid line is the prediction of Donnachie and Landshoff, normalized to lower energy data, using a supercritical pomeron[24]. It predicts a slower rise in cross section with W than is observed. This is also true of other VDM type models[3, 4]. The essential point of the QCD inspired models is that the cross section is proportional to the square of the gluon density. At the HERA energy ranges very low x values (from $\sim 5 \times 10^{-4}$ to 5×10^{-3} in the present analysis) contribute to J/ψ production. The shaded band in Fig. 4 is the prediction of the Ryskin model[5], obtained with DIPSI (with $\alpha_s = 0.25$), using the upper and lower limits of the leading order (LO) gluon momentum density as extracted by the ZEUS experiment[25] from the scaling violation of F_2 at $Q^2 = 7$ GeV^2 and evolved back to $Q^2 = 2.5$ GeV^2, the scale used in the model. The energy behaviour shown by the shaded band is in accord with the data. A recent modification by Ryskin[26], which uses a calculation based on the present model[5] and a gluon distribution with some saturation effects is also in agreement with our measurements; so is the calculation of Nemchik, Nikolaev and Zakharov[6], which uses the dipole cross section solution of the generalized BFKL [27] equation.

9 Conclusions

We have measured the elastic photoproduction cross section of J/ψ in ep interactions at γp c.m. energies between 40 and 90 GeV ($\langle W \rangle = 67$ GeV) and 90 and 140 GeV ($\langle W \rangle = 114$ GeV). The J/ψ was detected in its leptonic decay modes (e^+e^- or $\mu^+\mu^-$) in events where the scattered electron and proton were not observed. The elastic photoproduction cross sections, obtained from the combined electron and muon decay modes, are :

$$\begin{aligned} \sigma_{\gamma p \to \mathrm{J}/\psi \mathrm{p}} &= 52^{+7}_{-12} \pm 10\ nb \quad for\ \langle W \rangle = 67 \text{ GeV and} \\ \sigma_{\gamma p \to \mathrm{J}/\psi \mathrm{p}} &= 71^{+13}_{-20} \pm 12\ nb \quad for\ \langle W \rangle = 114 \text{ GeV}. \end{aligned}$$

The observed rise in the cross section compared to the lower energy measurements is not adequately described by Regge-type models and is better represented by perturbative calculations if a rise in the gluon density in the proton at low x is assumed.

10 Acknowledgement

We thank the DESY Directorate for their strong support and encouragement. The remarkable achievements of the HERA machine group were essential for the successful completion of this work, and are very much appreciated. We also gratefully acknowledge the support of the DESY computing and network group. Finally, we wish to thank N. N. Nikolaev and M. Ryskin for useful discussions.

References

[1] J.J. Sakurai, Phys. Rev. Lett. 22 (1969) 981.

[2] A. Donnachie and P.V. Landshoff, Nucl. Phys. B244 (1984) 322;
A. Donnachie and P.V. Landshoff, Nucl. Phys. B267 (1986) 690.

[3] E. Gotsman, E.M. Levin and U. Maor, CBPF-NF-025/94.

[4] H. Jung, G. Schuler and J. Terron, Int. J. Mod. Phys. A32 (1992) 7995.

[5] M. Ryskin, Z. Phys. C57 (1993) 89.

[6] J. Nemchik, N.N. Nikolaev and B.G. Zakharov, Phys. Lett. B341 (1994) 228.

[7] U. Camerini et al., Phys. Rev. Lett. 35 (1975) 483;
BPF Collab., A.R. Clark et al., Phys. Rev. Lett. 43, (1979) 187;
EMC Collab., J.J. Aubert et al., Nucl. Phys. B213, (1983) 1;
NA-14 Collab., R. Barate et al., Z. Phys. C33 (1987) 505;
E687 Collab., P.L. Frabetti et al., Phys. Lett. B316 (1993) 197;
NMC Collab., M. Arneodo et al., Phys. Lett. B332 (1994) 195.

[8] E401 Collab., M. Binkley et al., Phys. Rev. Lett. 48 (1982) 73;
E516 Collab., B. H. Denby et al., Phys. Rev. Lett. 52 (1984) 795.

[9] H1 Collab., T. Ahmed et al., Phys. Lett. B338 (1994) 507.

[10] ZEUS Collab., The ZEUS Detector, Status Report, DESY (1993).

[11] C. Alvisi et al., Nucl. Instr. and Meth. A305 (1991) 30.

[12] N. Harnew et al., Nucl. Instr. and Meth. A279 (1989) 290;
C.B. Brooks et al., Nucl. Instr. and Meth. A283 (1989) 473;
B. Foster et al., Nucl. Phys. B, Proc. Suppl. B32 (1993) 181;
B. Foster et al, Nucl. Instr. and Meth. A338 (1994) 254.

[13] M. Derrick et al., Nucl. Instr. and Meth. A309 (1991) 77;
A. Andresen et al., Nucl. Instr. and Meth. A309 (1991) 101;
A. Bernstein et al., Nucl. Instr. and Meth. A336 (1993) 23.

[14] G. Abbiendi et al., Nucl. Instr. and Meth. A333 (1993) 342.

[15] M. Arneodo, L. Lamberti and M. Ryskin, to be submitted to Comp. Phys. Comm.

[16] H. Jung, Proc. of the Workshop 'Physics at HERA', Vol III., Oct 1991, p. 1488;
H. Jung et al., Z. Phys. C60 (1993) 721.

[17] S.P. Baranov et al., Proc. of the Workshop 'Physics at HERA', Vol III., Oct 1991, p. 1478.

[18] T. Sjöstrand and M. Bengtsson, Comp. Phys. Comm. 43 (1987) 367;
H.U. Bengtsson and T. Sjöstrand, Comp. Phys. Comm. 46 (1987) 43.

[19] CDF Collab., F. Abe et al., Phys. Rev. D50 (1994) 5535.

[20] G.A. Schuler and T. Sjöstrand, CERN-TH.6796/93 and references therein.

[21] G. Marchesini et al., Comp. Phys. Com. 67 (1992) 465;
B.R. Webber, Proc. of the Workshop 'Physics at HERA', Vol III., Oct 1991, p. 1354;
L. Stanco, ibidem, p. 1363.

[22] Particle Data Group, L. Montanet et al., Phys. Rev. D50 (1994) 1664.

[23] V.N. Gribov et al., Sov. Phys. JETP 14 (1962) 1308;
V.M. Budnev et al., Phys. Rep. C15 (1975) 181.

[24] A. Donnachie and P.V. Landshoff, DAMTP 94/99, hep-ph 9411368 (1994).

[25] ZEUS Collab., M. Derrick et al., DESY 94-192, accepted by Phys. Lett. B.

[26] M. Ryskin, Surveys in High Energy Physics, 7 (1994) 137 and private communication.

[27] Y. Balitskij and L.N. Lipatov, Sov. J. Nucl. Phys. 28 (1978) 822;
E. Kuraev, L.N. Lipatov and V.S. Fadin, Sov. Phys. JETP 44 (1976) 443.

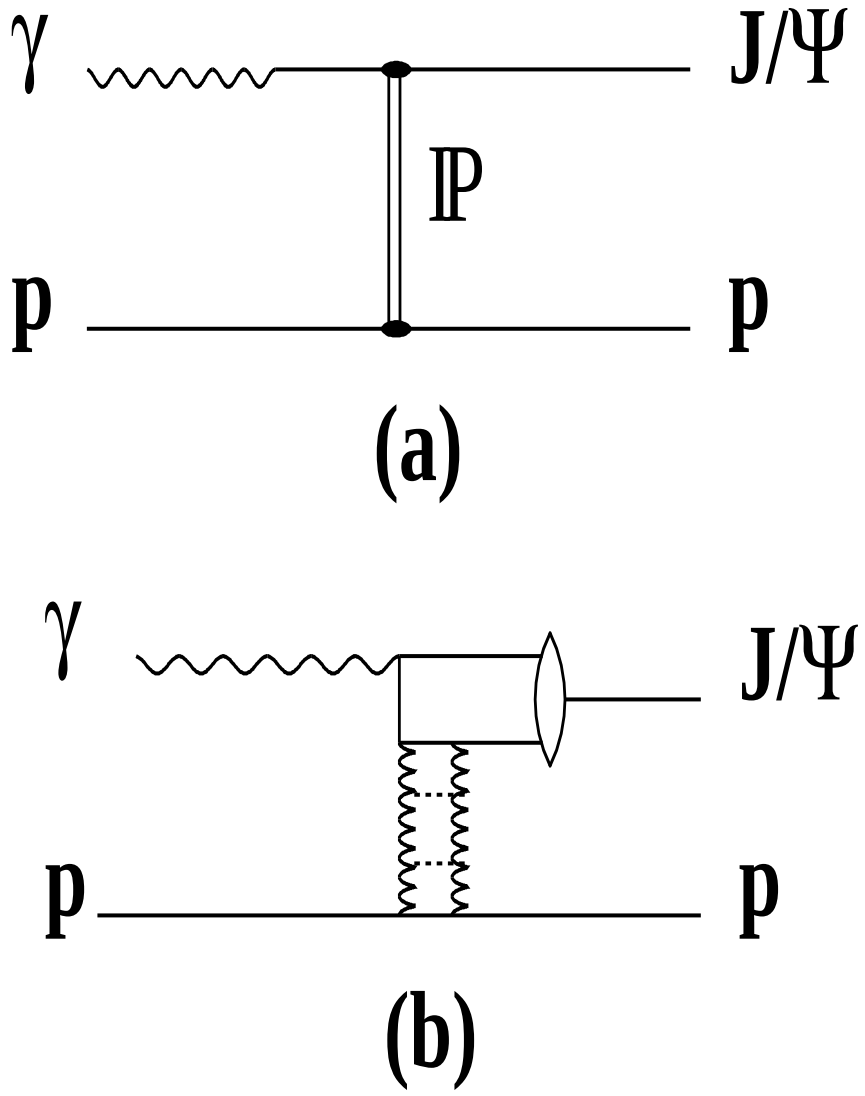

Figure 1: A schematic diagram of elastic J/ψ production according to (a)VDM with a pomeron exchange and (b) QCD-inspired models with the exchange of a gluon ladder.

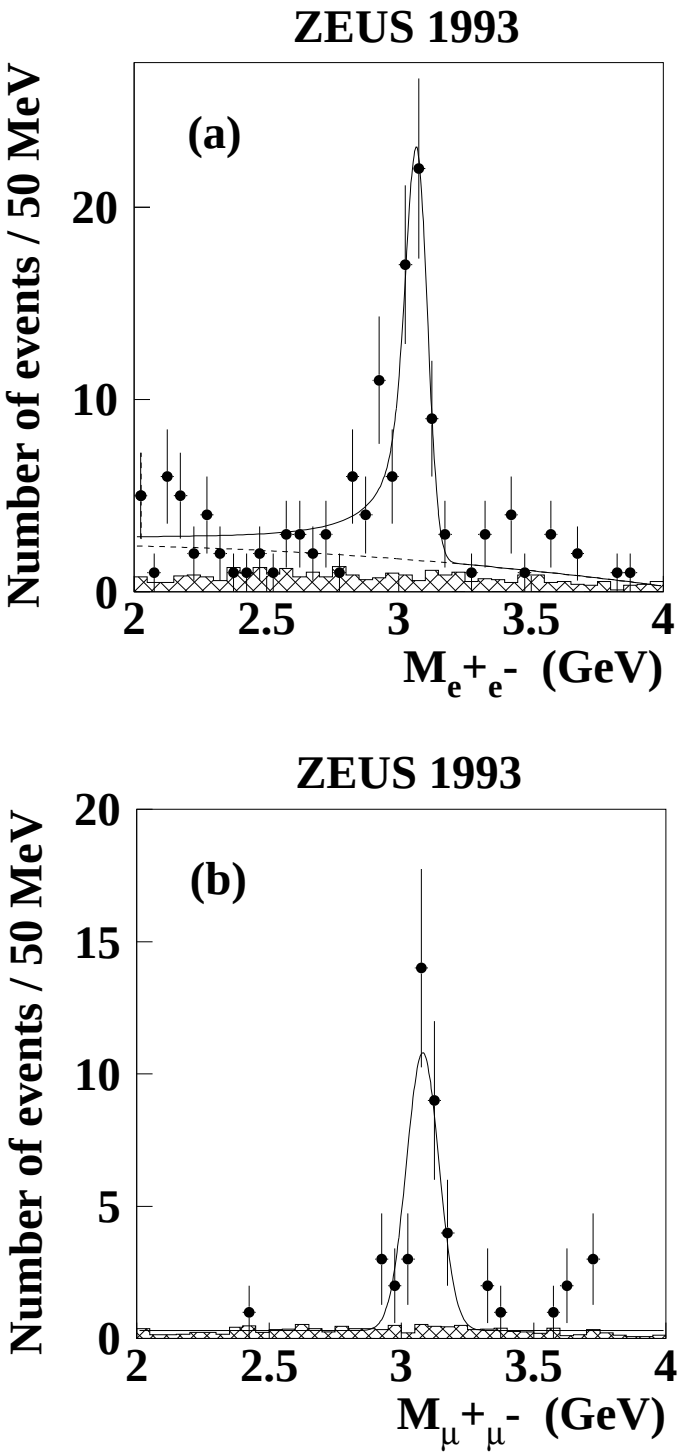

Figure 2: (a) The reconstructed e^+e^- invariant mass spectrum for $40 \leq W \leq 140$ GeV. The solid circles represent the data; the solid line indicates a fit to the data with the convolution of a Gaussian and a bremsstrahlung function; the dotted line represents a quadratic polynomial parametrising the background; the shaded area is the expected contribution from the two-photon background. (b) The reconstructed $\mu^+\mu^-$ invariant mass spectrum for $40 \leq W \leq 140$ GeV. The solid circles represent the data; the solid line indicates a fit with a Gaussian and a flat background. The shaded area shows the flat background expected from the two-photon process.

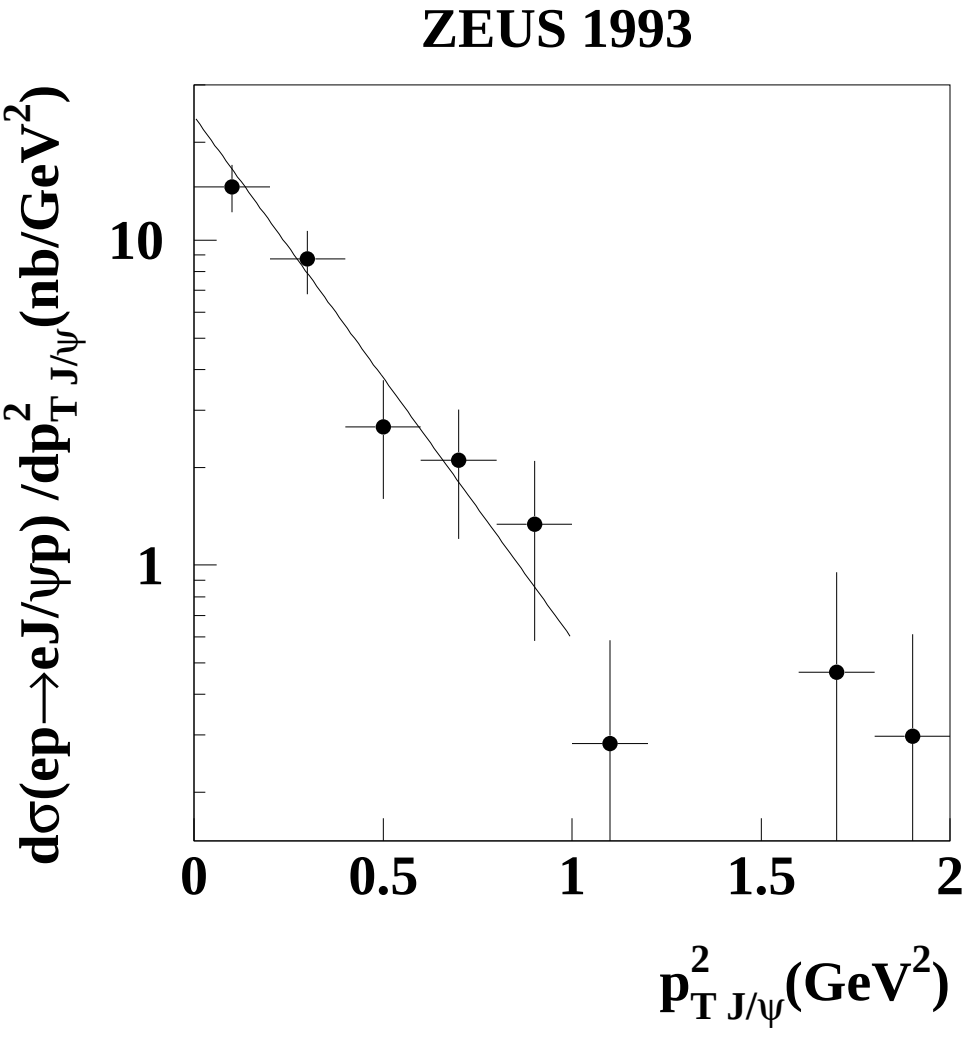

Figure 3: the differential cross section $d\sigma_{ep}/dp^2_{T\mathrm{J}/\psi}$ for $\mathrm{e}^-\mathrm{p} \to \mathrm{e}^-\mathrm{J}/\psi$ p from both decay channels combined for $40 \leq W \leq 140$ GeV. The continuous line indicates the result of a fit with the function $\exp(-bp^2_{T\mathrm{J}/\psi})$ with $b = 3.7 \pm 1.0$ GeV^{-2}. Only statistical errors are shown.

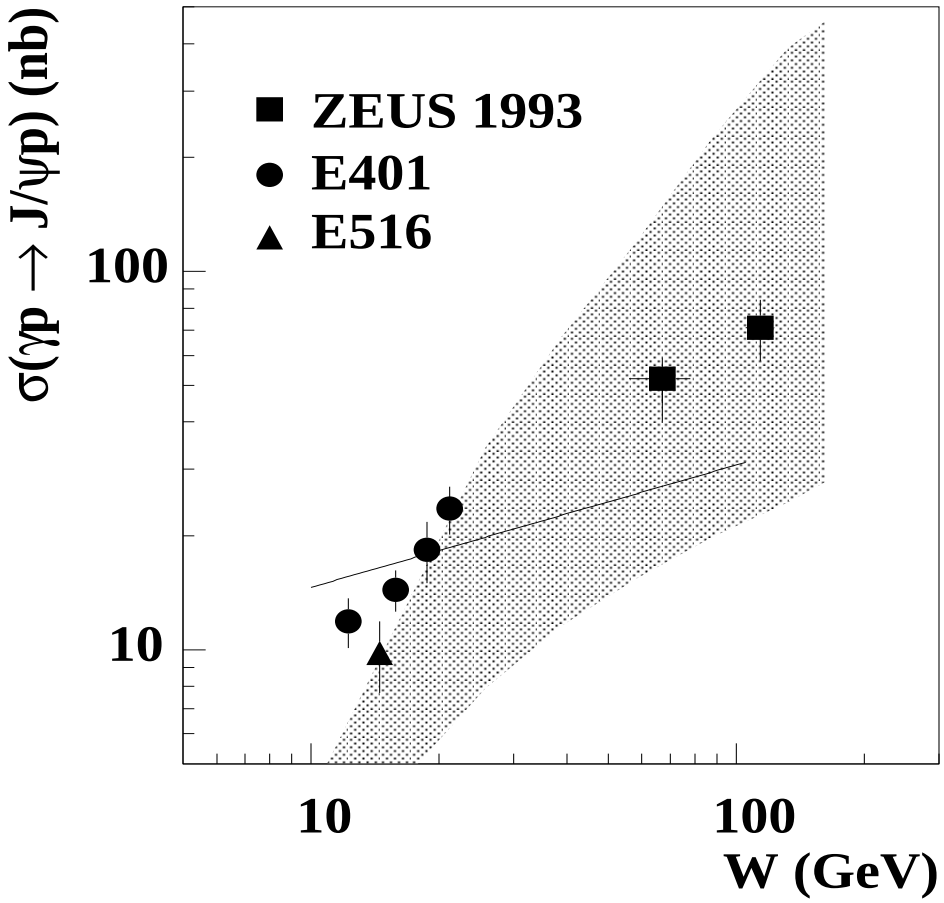

Figure 4: A compilation of J/ψ elastic cross sections in photoproduction. The solid squares represent the measurements from the ZEUS experiment at $\langle W \rangle$ values of 67 GeV and 114 GeV. The shaded region represents the prediction of the Ryskin model[5] using the upper and lower limits of the gluon momentum density as extracted by the ZEUS experiment at $Q^2 = 7$ GeV^2[25] in LO and evolved back to 2.5 GeV^2. The solid line is a VDM-like prediction[24].